CrystEngComm

Accepted Manuscript

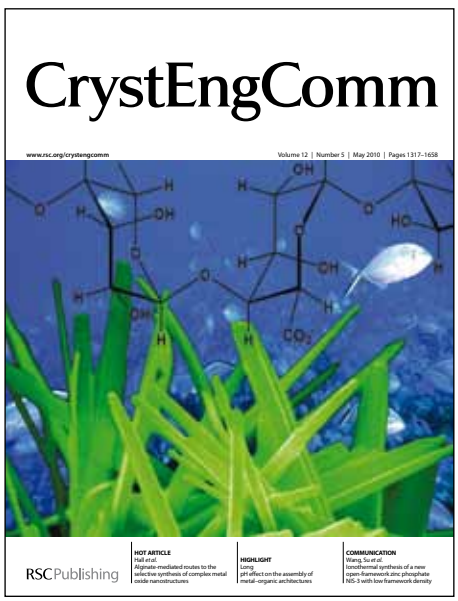

CrystEngComm

RSCPublishing

ARTICLE

www.rsc.org/

A new synthetic route to hollow Co_3O_4 octahedra for supercapacitor applications

Yuebin Cao,[a,&] Fangli Yuan,[b,&] Mingshui Yao,[b] Jin Ho Bang[c,*] and Jung-Ho Lee[a,*]

Co_3O_4 hollow octahedra were successfully synthesized via a facile one-step solvothermal route. Time-resolved electron microscopy and X-ray diffraction analyses revealed that the Co_3O_4 hollow octahedra were formed through the self-assembly of primary nanocrystals followed by subsequent Ostwald ripening. Subtle control over the reaction conditions led to different morphologies (hexagonal plates and nanocubes) and crystal structures (β-$Co(OH)_2$/Co_3O_4 composite). The unique hollow nanostructure rendered our Co_3O_4 potentially useful for charge-storage applications. To prove its usefulness, the pseudocapacitive performance of the Co_3O_4 hollow octahedra as a supercapacitor electrode was evaluated, and exhibited a charge storage capacity of 192 F g^{-1} with good long-term cyclability.

INTRODUCTION

Supercapacitors have received increasing attention as next-generation energy storage devices because of their high power densities, fast charge-discharge rate, long cycling life, and safe operation.[1] Based on the charge storage mechanism, supercapacitors can be divided into electric double-layer capacitors and pseudocapacitors. Pseudocapacitors, where charges are stored through fast and reversible surface faradic redox reactions, have higher specific capacitance than electric double-layer capacitors that store charges at the electrode-electrolyte interface. Transition metal oxides and hydroxides are found to be excellent pseudocapacitive materials because of various oxidation states possessing for charge transfer. RuO_2 stands out for its excellent pseudocapacitive performance, but the high cost of RuO_2 has hindered its practical application.[2] Countless efforts have been dedicated to the development of cost-effective pseudocapacitive materials whose performance is comparable to that of RuO_2. Among various candidates (NiO,[3] $Ni(OH)_2$,[4] MnO_2,[5] V_2O_5,[6] etc.[7]), Co_3O_4 is considered to be one of the most attractive materials due to its good redox activity and high theoretical specific capacitance (3560 F g^{-1}).[8] For high-performance supercapacitors, it is critical to possess a sufficiently large electroactive surface for the faradic redox reaction and to enhance the kinetics of ion and electron transport on the electrodes and the electrode-electrolyte interface. To meet such requirements, a wide variety of nanostructured Co_3O_4 morphologies, including nanowires,[9] hollow structures,[10] nanoplates,[11] and porous cubes,[12] have been investigated.

In particular, hollow micro/nano-structured materials have proven their prowess in energy storage system applications (Li-ion batteries[13] and supercapacitors[14]) due to their exceptional interior geometry and shell functionality. Such a unique structure not only increases the contact area between the electrolyte and active material, but also facilitates mass and charge transport. In general, the synthesis of hollow structures is involved in a template method, in which desired materials or their precursors are deposited onto various templates (SiO_2, carbon spheres, polymer, etc.) and the removal of these sacrificial templates by chemical etching or thermal decomposition yields hollow nanostructures.[15] Various hollow Co_3O_4 structures such as nanospheres, nanotubes, and nanoboxes, have been successfully fabricated via the template method by using polystyrene, porous anodic alumina membranes, or dodecylbenzenesulfonate as templates.[10b,13d,16] However, the template method suffers from high cost and a tedious synthetic procedure, which has urged scientists to develop template-free approaches. For example, Au et al. reported the synthesis of Co_3O_4 nanotubes via a modified Kirkendall effect.[17] Xue and coworkers synthesized anisotropic Co_3O_4 hollow nanocapsules derived from a $CoCO_3$ precursor, the formation of which was explained by the Ostwald ripening mechanism.[13e]

In this work, we report a facile solvothermal method to prepare Co_3O_4 hollow octahedra without using any templates. Our in-depth analysis of the reaction intermediates revealed that the self-assembly of primary nanoparticles and the following Ostwald ripening led to the formation of Co_3O_4 hollow octahedra. As far as we know, it is the first report of hollow Co_3O_4 octahedra synthesized through template-free methods. In addition to the hollow octahedra, we were able to synthesize Co_3O_4 nanocubes with edge lengths of 20–50 nm by simply changing the cobalt precursor from $CoCl_2$•$6H_2O$ to $Co(CH_3COO)_2$•$4H_2O$. The newly prepared Co_3O_4 hollow nanostructures were evaluated as an active material for a pseudocapacitor. Our study found that the Co_3O_4 hollow octahedra exhibited a higher specific capacitance than the

Co_3O_4 nanocubes because of lower series and diffusive resistances of the Co_3O_4 octahedra.

EXPERIMENTAL SECTION

Preparation of Co_3O_4 hollow octahedra

In a typical preparation, $CoCl_2 \cdot 6H_2O$ (0.2 mmol) was dissolved in a mixed solvent of ethanol and de-ionized water (20 mL) with a volume ratio of 2:1. NaOH (0.02 mol) was then added to the cobalt chloride solution under stirring in air. Dark brown CoOOH nanoparticles were formed after 30 min of stirring. The CoOOH suspension was transferred into a 50 mL Teflon-lined stainless steel autoclave and heated at 200 °C for 4 h. After the reaction, the product was collected and washed with de-ionized water and ethanol several times to remove impurities.

Characterization

The crystal structure of products was examined with an X-ray diffractometer (X' pert PRO, PANalytical, Cu Kα radiation) operated at 40 kV and 30 mA. The size and morphology of the products were analyzed with a transmission electron microscope (TEM, JEOL JEM-2010) and a field-emission scanning electron microscope (FE-SEM, Hitachi S-4800).

Electrochemical measurements

Working electrodes were prepared by a drop-casting method. For suspension preparation, 80 wt% of electroactive material (Co_3O_4), 15 wt% of carbon black (Ketjen black), and 5 wt% of polyvinylidene difluoride were mixed thoroughly with a small amount of ethanol. Sonication of this mixture for 10 min led to a homogeneous suspension. The suspension was then dropped onto a piece of carbon fiber paper (1 cm × 2 cm) and dried at 50 °C overnight. The loading of Co_3O_4 on the carbon fiber paper was 0.5 mg cm^{-2}. To determine the contribution of carbon black to the overall capacitance, an electrode was prepared in a similar fashion without adding Co_3O_4.

The electrochemical performance of the electrodes was evaluated with an IviumStat electrochemical workstation. Cyclic voltammetry (CV) and chronopotentiometry measurements were carried out in a three-electrode electrochemical cell with a Pt foil counter electrode and an Ag/AgCl reference electrode in a 2 M KOH aqueous electrolyte. The electrochemical impedance spectroscopy (EIS) was performed in a two-electrode electrochemical cell with a frequency range of 0.1 to 100 kHz and a perturbation amplitude of 10 mV. In the two-electrode electrochemical cell, two identical Co_3O_4 electrodes served as the working electrode and counter electrode, respectively.

RESULTS AND DISCUSSION

The structure and morphological characterizations of the reaction product are shown in Figure 1. Figure 1a displays a typical X-ray diffraction (XRD) pattern of the product. All the diffraction peaks are in good accordance with the spinel Co_3O_4 phase (JCPDS 42-1467), and the intensity of the peaks indicates the high crystallinity of the Co_3O_4 product. No peaks from possible impurities were detected, implying that the Co_3O_4 was pure. Figure 1b exhibits a low-magnification SEM image of the as-prepared Co_3O_4, which shows that the Co_3O_4 was a regular octahedra with edge lengths ranging from 500 nm to 1 μm. A high-resolution SEM image of these octahedra revealed that the Co_3O_4 octahedra were composed of aggregated and fused particles with sizes of tens to hundreds nanometers (Figure 1c). A broken octahedron shown in the inset of Figure 1c indicates that the interior of the Co_3O_4 octahedra was not solid but hollow. Other SEM images of the broken octahedra are shown in Figure S1 in Supporting Information. The TEM image of these Co_3O_4 octahedra, as shown in Figure 1d, further supported the formation of hollow structure. The selected area electron diffraction (SAED) pattern of a hollow octahedron in the inset of Figure 1d revealed that the octahedron was single crystalline, which implies that a substantial number of crystallites in the sample were crystallographically oriented.

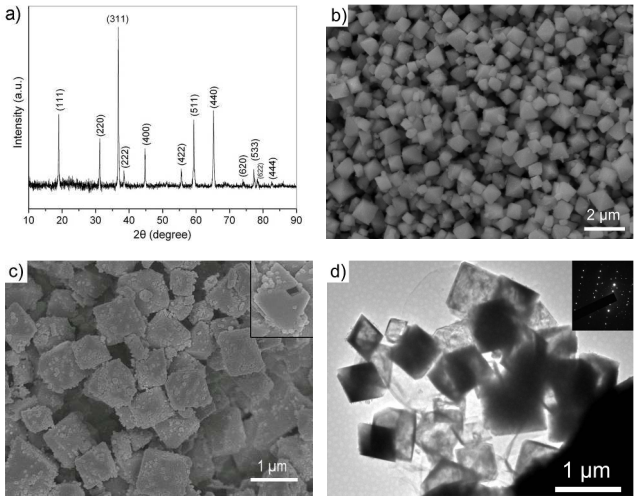

Figure 1. (a) XRD pattern, (b) low-magnification SEM image, (c) high-magnification SEM image (inset: SEM image of a broken octahedron), and (d) TEM image (inset: SAED of a octahedron) of Co_3O_4 octahedra obtained after solvothermal reaction at 200 °C for 4 h.

To investigate the formation mechanism of the Co_3O_4 hollow octahedra, the reaction intermediates obtained at different reaction times were characterized with XRD, SEM, and TEM. Figure 2a shows the XRD pattern of the precursor for the solvothermal reaction which was collected after adding NaOH into the cobalt chloride solution and stirred for 30 min. The main XRD diffraction peaks match that of the cobalt oxyhydroxide, CoOOH (JCPDS 07-169). The broad and low intensity of the diffraction peaks revealed the poor crystallinity of the obtained CoOOH. Two small, sharp peaks at 36.5° and 65° may be ascribed to Co_3O_4, which are the two primary diffraction peaks of Co_3O_4. This suggests that a small amount Co_3O_4 may be formed in the drying process prior to the XRD measurement.

The SEM image of the CoOOH precursor (Figure 3a) shows that the CoOOH consisted of irregularly-shaped nanoparticles. After a 1.5 h reaction, intense diffraction peaks from Co_3O_4 started to appear, and only a weak CoOOH peak at ~20° was preserved, indicating that most of the CoOOH was transformed to Co_3O_4 (Figure 2b). The corresponding SEM and TEM images revealed that the Co_3O_4 consisted of dispersed nanocrystals with sizes ranging approximately tens of nanometers (Figure 3b). When the reaction time was further increased to 2 h, the diffraction peak of CoOOH disappeared and only Co_3O_4 diffraction peaks remained, which indicated that the CoOOH was completely transformed to Co_3O_4 (Figure

2c). From the corresponding SEM image (Figure 3c) and TEM images (the inset of Figure 3c and Figure S2), it can be inferred that quasi-octahedra were formed through the assembly of primary nanoparticles. Besides the quasi-octahedra, some dispersed nanoparticles were still seen in the product, indicating that self-assembly was still underway.

When reaction time was extended to 4 h, the dispersed Co_3O_4 nanoparticles disappeared, and regular Co_3O_4 hollow octahedra assembled with recognized primary nanoparticles were formed (Figure 3d). The XRD peaks became more intense than that of the intermediates obtained after 2 h, indicating that the crystallinity improved and the crystallite size became larger (Figure 2d). After 12 h, the surfaces of these octahedra became smooth, and no primary nanoparticles were recognized, as shown in Figure 3e. These octahedra, however, still retained the hollow structure as confirmed by TEM (the inset of Figure 3e). The XRD pattern of the sample showed a more intense array diffraction peaks compared to that of the Co_3O_4 obtained after 4 h reaction (Figure 2e). Surprisingly, when the reaction was extended to 24 h, most of the hollow octahedra were transformed to hexagonal plates with an edge length of more than ten micrometers, and only a few of the octahedra were preserved (Figure 3f). The XRD pattern of the hexagonal plates showed a much higher peak ratio of (111) to (311), which implies that the {111} planes were preferentially formed during the reaction (Figure 2f).

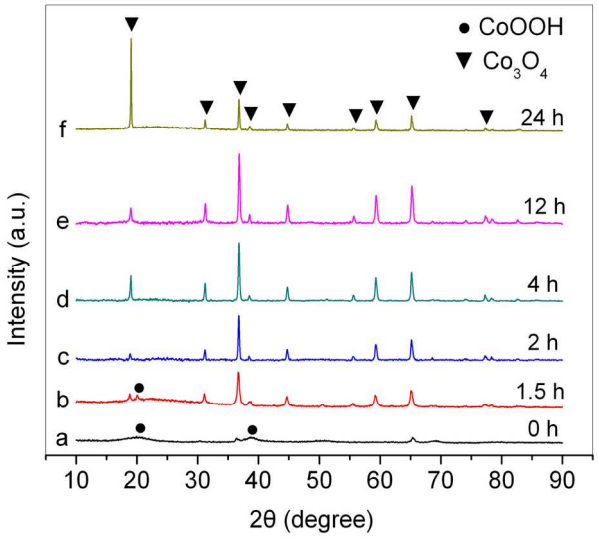

Figure 2. XRD patterns of the products obtained at different reaction times: (a) 0 h, (b) 1.5 h, (c) 2 h, (d) 4 h, (e) 12 h, and (f) 24 h.

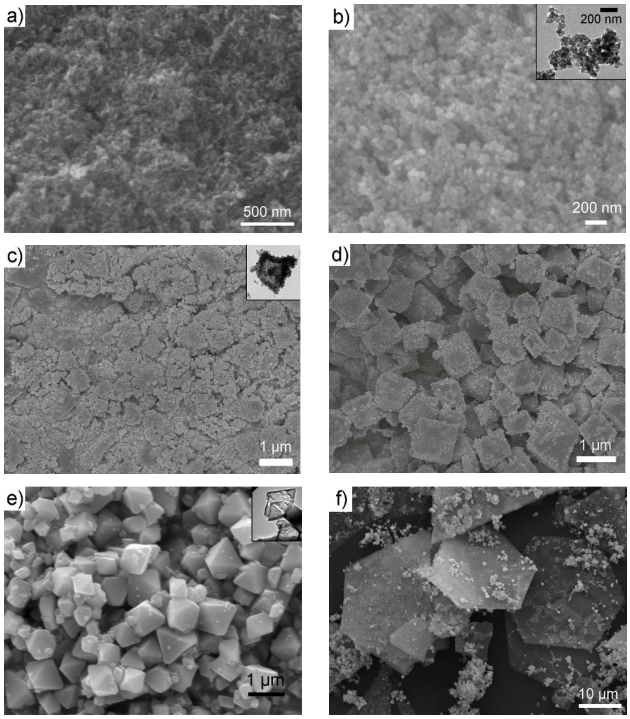

Figure 3. SEM and TEM images of the products obtained at different reaction times: (a) 0 h, (b) 1.5 h, (c) 2 h, (d) 4 h, (e) 12 h, and (f) 24 h. Insets in Figure 3b, 3c, and 3e are their corresponding TEM images.

On the basis of our observations, the structural and geometrical evolution that occurred in the solvothermal process is proposed in Scheme 1. As soon as NaOH was added into the cobalt chloride solution, $Co(OH)_4^{2-}$ was initially formed as indicated by the quick color change of the solution from pink to blue. After being stirred for 30 min, Co (II) was gradually oxidized by O_2 dissolved in an ethanol/water solvent to dark brown CoOOH because CoOOH was stable in the solution due to the excellent stability of Co (III) under alkaline conditions.[18] The CoOOH nanoparticles were then gradually transformed to Co_3O_4 nanoparticles under solvothermal conditions at 200 °C (Step 1). There are several reports on the thermal decomposition of CoOOH to Co_3O_4; in these cases the conversion required a heating temperature above 200 °C. For instance, the decomposition temperature of CoOOH determined by thermal gravimetry was 244–312 °C according to Avramov's study;[19] the decomposition temperature reported by Kittaka *et al.* was 220–260 °C;[20] and the decompostion temperature reported by Suib *et al.* was 250–300 °C.[21] Thus, it is not likely that the Co_3O_4 was formed by the thermal decomposition of CoOOH in our case as the solvothermal treatment was performed at 200 °C. It is well-known that ethanol can serve as a reducing agent in a hot basic solution, thus it plays this role in the synthesis of Cu, Ag, Au, Pd, and Ni.[22] Therefore, we speculate that our Co_3O_4 may be formed via the reduction of CoOOH by ethanol as a reducing agent. In the initial reduction process, Co (III) in CoOOH was partially reduced to Co (II). The reduced Co (II) may exist as $Co(OH)_4^{2-}$ because of the fairly high OH^- concentration used in our synthesis. Then $Co(OH)_4^{2-}$ reacted with CoOOH nanoparticles to form Co_3O_4 as suggested in equation (1), which is similar to the reaction mechanism proposed by Formaro and coworkers.[23]

$$Co(OH)_4^{2-} + 2CoOOH \rightarrow Co_3O_4 + 2OH^- + 2H_2O \quad (1)$$

Control experiments provided indirect evidence for our proposed mechanism. When the NaOH concentration was doubled to 2 M, a composite of pink β-$Co(OH)_2$ and black Co_3O_4 were obtained after 2 h instead of Co_3O_4. Even when the reaction time was prolonged to 24 h, the same composite was obtained. Figure S3 exhibits the XRD and SEM images of the β-$Co(OH)_2$/Co_3O_4 composite obtained after 24 h reaction. With the high NaOH concentration, the reduction capacity of the solution was substantially enhanced, thus the Co (III) in CoOOH could be reduced to Co (II) more quickly. Since CoOOH was consumed at a higher rate, the resulting $Co(OH)_4^{2-}$ may have less chance to react with CoOOH to form Co_3O_4. As a result, a large amount of Co species exist as Co (II) after CoOOH was depleted. This accounts for the formation of the β-$Co(OH)_2$/Co_3O_4 composite at a high NaOH concentration.

In addition, we found that the solution volume filled in the autoclave also has a substantial influence on the crystal structure of the products. When the autoclave was filled with 30 mL of reaction solution, rather than 20 mL (*i.e.,* the air volume sealed in the autoclave decreased from 30 to 20 mL), the solvothermal reaction yielded the β-$Co(OH)_2$/Co_3O_4 composite instead of pure Co_3O_4. It is reasonable to deduce that the volume of O_2 sealed in the autoclave, which was related to the amount of dissolved O_2 in the solution, affected the final products. A similar effect of O_2 on the crystal phases of cobalt oxide was observed by Zhang and coworkers.[24] We speculate that the amount of dissolved O_2 can precisely control the reduction ability of the solution. In the case of the 30 mL-filled solution, the sealed O_2 and corresponding dissolved O_2 in solution decreased, thus improving the reduction ability of the solution compared to that of the 20 mL-filled solution. As in the situation with the use of a high NaOH concentration, such improved reduction ability was capable of inducing the formation of the β-$Co(OH)_2$/Co_3O_4 composite. Our control experiments suggested that the production of pure Co_3O_4 required a delicate control of the experimental conditions.

In Step 2, the Co_3O_4 nanoparticles become self-assembled to form quasi-octahedra. In general, nanoparticles possess large surface area and high surface energy, thus having a strong tendency towards aggregation in order to reduce excess energy. Recent studies have illustrated that particle-mediated aggregation is one of the most important crystal growth processes, which can lead to the formation of highly ordered particle assemblies known as "mesocrystals".[25] In the classical crystallization, crystal growth in the solution in the absence of surfactants is based on thermodynamic equilibrium, thus the crystal shape is mainly dictated by facets having the lowest surface energy. It has been proven that this rule also applies when the growing units are nano or meso-crystals.[26] For a face-centered cubic (fcc) crystal structure, the surface energies (γ) of the low-index crystallographic facets is given in the order of $\gamma\{111\} < \gamma\{100\} < \gamma\{110\}$.[27] Therefore, the primary Co_3O_4 nanoparticles have a strong tendency to become self-assembled to the octahedral morphology that possesses six {111} faces.

The quasi-spherical Co_3O_4 nanoparticles (Figure 3b) can be regarded as small crystals enclosed by various low-index faces ({110}, {100}, and {111}). Driven by Brownian motion, nanocrystals suspended in solution randomly collided to form aggregates; moreover, it is believed that, after aggregation, the adjacent nanocrystals can rotate to find a low-energy configuration owing to Brownian motion and short-range interactions between adjacent surfaces.[28] Thus, it is reasonable to infer that the relatively higher energy planes such as {110} and {100} were eliminated by oriented attachment during this process, and as a result, only the lowest energy planes {111} were preserved.

In Step 3, the core region of the assembled quasi-octahedra was dissolved, and the hollow octahedra were formed along with shells densely assembled with nanoparticles. Based on our time-resolved experiments, Ostwald ripening is estimated to play a crucial role in the formation of the hollow structure.[29] Formation of hollow interiors stems from mass transfer between the solid core and outside chemical solution through nano-channels between nanoparticles. Compared to those in the outer surfaces, the crystallites located in the inner cores have high surface energies because they can be regarded as a smaller particle having a higher curvature (*i.e.*, higher surface energies are more readily dissolved). As a result, the inner nanocrystallites of an octahedron were dissolved, followed by re-crystallization on the outer nanocrystallites of the octahedron to reduce the surface energy. During this process, crystallinity was improved, as identified in the XRD analysis, which supported the Ostwald ripening mechanism.

In Step 4, the primary nanocrystals that compose the octahedra shell coalesced, and the octahedra surfaces became smooth, indicating that the shell became transformed from mesocrystals to single crystals. Such coalescence of primary nanoparticles to form smooth surfaces is ascribed to the mass transfer from nanoparticles surfaces to the neck region between nanoparticles, as noted in previous studies.[30] In the last step, the Co_3O_4 hollow octahedra were transformed to hexagonal plates after a 24 h solvothermal treatment. It is still unclear why the Co_3O_4 became transformed to a hexagonal plate. We speculate that it may be because the hexagonal plates possess a lower surface energy than the hollow octahedra owing to the larger size of hexagonal plates, although both the hexagonal plate and octahedron expose the same low energy {111} planes.

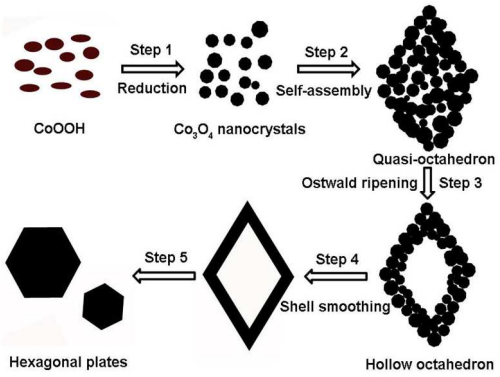

Scheme 1. Structural and geometrical evolution during the solvothermal reaction.

Cobalt salts used as a precursor were found to have additional effect on the Co_3O_4 morphology. When $Co(CH_3COO)_2 \cdot 4H_2O$ was used instead of $CoCl_2 \cdot 6H_2O$, Co_3O_4,

nanocubes were obtained. Figure 4a shows the XRD pattern of the nanocubes, confirming the formation of pure Co_3O_4. SEM and TEM images of the Co_3O_4 nanocubes were shown in Figure 4b and 4c, respectively, indicating that the final product was well-dispersed nanocubes with edge lengths of 20–50 nm. The high resolution transmission electron microscopy (HRTEM) image of the nanocubes shown in Figure 4d reveals that the lattice spacings of 0.289 and 0.232 nm are in good agreement with the interplanar spacings of {220} and {222} planes of spine Co_3O_4. The direction perpendicular to the cube surface can be indexed as [1–10]. Therefore, the exposed crystal planes for these nanocubes were determined to be {110}. The role of acetate ions in the morphology-controlled synthesis of nanocrystals has been demonstrated in terms of their selective adsorption on crystal planes.[31] In our case, the formation of nanocubes enclosed with {110} planes implies that the acetate ion may be adsorbed preferentially on {110} planes, thus lowering the energy of {110} planes.

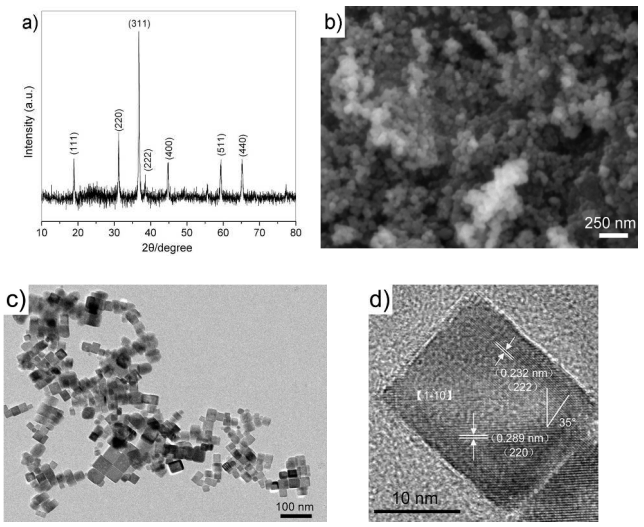

Figure 4. (a) XRD pattern, (b) SEM and (c) TEM images of Co_3O_4 nanocubes; (d) HRTEM of a Co_3O_4 nanocube.

The hollow Co_3O_4 octahedra possess void interior space. As they are assembled with nanocrystallites, the contact area between the electrolyte and Co_3O_4 would be large, which is desirable for efficient redox reactions in pseudocapacitor applications. For the sake of comparison, the capacitive performances of Co_3O_4 nanocubes and of hexagonal plates were evaluated. Figure 5a shows the cyclic voltamograms (CVs) of Co_3O_4 hollow octahedra at scan rates of 5–50 mV s^{-1}. The obvious reduction and oxidation peaks indicate that the charge storage of the electrode mainly resulted from pseudocapacitance and not from the electrical double layer capacitance. Two current peaks were observed at ~0.42 V and ~0.22 V during the cathodic sweep (at the low scan rates of 5 and 10 mV s^{-1}), which corresponds to the conversion between different cobalt oxidation states (equations 2 and 3). The two oxidation peaks merged together leaving one broad oxidation peak at ~0.45 V.

$$Co_3O_4 + OH^- + H_2O \leftrightarrow 3CoOOH + e- \quad (2)$$

$$CoOOH + OH^- \leftrightarrow CoO_2 + H_2O + e- \quad (3)$$

The symmetric characteristic of the anodic and cathodic peaks indicates a good redox reversibility of the Co_3O_4 hollow octahedra electrode. Moreover, the anodic/cathodic peak current density of the electrode increased quasi-linearly with the potential scan rate, revealing its excellent reactivity. Figure 5b shows the CV curves of various Co_3O_4 electrodes measured at a scan rate 10 mV s^{-1}. The CV curve of carbon black used as a conductive agent for the Co_3O_4 electrodes is also shown in Figure 5b. The specific capacitance is known to be proportional to the integral area of the CV curves.[1d] The Co_3O_4 hollow octahedra electrode shows the highest integral area in comparison with Co_3O_4 nanocubes and hexagonal plates, indicating its highest specific capacitance. The carbon black shows the smallest integral area, implying that the contribution of carbon black to the total capacitance is negligible.

The specific capacitances of the Co_3O_4 electrodes were obtained by constant current charge-discharge tests in the potential range between –0.05 V and 0.45 V. Figure 5c shows the discharge curves of various Co_3O_4 electrodes at a constant current density of 1 A g^{-1}. The discharge curve of carbon black was a straight line, showing a characteristic typical of an electric double-layer capacitor. On the contrary, non-straight curves were observed for the Co_3O_4 electrodes, indicating that faradic redox reactions are responsible for the charge storage. The specific capacitances were calculated according to the following equation:

$$C_m = I \times \Delta t / \Delta V \times m \quad (4)$$

where C_m (F g^{-1}) is the specific capacitance, I (A) is the applied current, Δt (s) is the time taken during discharge, ΔV is the voltage window, and m (g) is the mass of the active material. The calculated specific capacitance of carbon black was only 2 F. After subtracting the capacitance of carbon black, the calculated specific capacitance of the Co_3O_4 hollow octahedra was 98 F g^{-1}, which was larger than those of Co_3O_4 nanocubes (70 F g^{-1}) and of hexagonal plates (15 F g^{-1}). The poor specific capacitance of the Co_3O_4 hexagonal plates can be easily rationalized because of its larger size (Figure 3e). To elucidate the difference in the specific capacitance of hollow octahedra and nanocubes, an electrochemical impedance spectroscopy (EIS) experiment was conducted. EIS can provide information of electrical conductivity and ion transfer ability of the electrode.

The Nyquist plots in Figure 5d show that the equivalent series resistances determined by the *x*-intercept of the Nyquist plots differed in the hollow octahedra and nanocubes electrodes. The resistances were found to be 3.6 Ω and 5.3 Ω for the hollow octahedra and the nanocubes electrode, respectively. This suggests that the hollow octahedra enabled high electron mobility through the electrode, which facilitates the transfer of electrons. Moreover, there was a difference in the linear responses in the low-frequency region, which represents an interfacial diffusive resistance. The hollow octahedra electrode exhibited less deviation from the imaginary axis than the nanocubes electrode, indicating that the hollow octahedra electrode has a lower diffusive resistance than the nanocubes electrode. Given these observations, the higher specific capacitance of the Co_3O_4 hollow octahedra electrode can be attributed to its lower series and diffusive resistance.

Figure 5e shows the discharge curves of a Co_3O_4 hollow ocrahedra electrode measured at different current densities. The discharge curves measured at lower current densities (1 and 2 A g^{-1}), can be divided into two stages, 0.45 V to 0.15 V and 0.15 V to 0.05 V. The linear discharge curve that appeared in the latter stage is ascribed to the electric double layer capacitance behavior of the electrode. For the former stage, a non-linear discharge curve was observed, which arose mainly from the faradic capacitance. Furthermore, the non-linear discharge curve exhibited two discharge plateaus which resulted from the conversion between different Co oxidation states according to equations 2 and 3. The characteristics of the discharge curves were consistent with the CV test. The specific capacitances of the Co_3O_4 hollow octahedra electrode as a function of current densities are shown in Figure 5f. It was found that the specific capacitances decreased as the current densities increased. The low specific capacitances found at high current densities were attributed to the limited access of electrolyte into Co_3O_4.

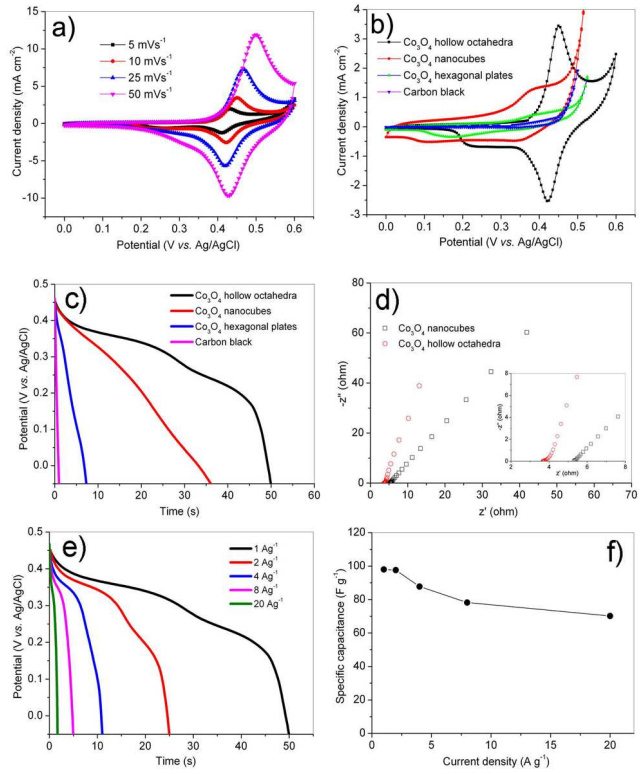

Figure 5. (a) CV curves of Co_3O_4 hollow octahedra electrode at different scan rates; (b) CV curves of various Co_3O_4 electrodes and carbon black electrode at scan rate 10 mV s^{-1}; (c) discharging curves of various Co_3O_4 electrodes and carbon black electrode at the discharging current of 1 A g^{-1}; (d) Nyquist plots of Co_3O_4 hollow octahedra and nanocubes electrodes (inset: enlarged spectra in high frequency region); (e) discharging curves and (f) corresponding specific capacitances of the Co_3O_4 hollow octahedra electrode at different discharging currents.

Figure S4 compares the discharge curves of the electrodes, in which the samples were fabricated with a variety of reaction times. Note that the CoOOH electrode for 0 h (Figure 2a, 3a) exhibited the highest specific capacitance (104 F g^{-1}) out of all the samples. CoOOH has been investigated as a promising supercapacitor material owing to its good electrical conductance.[32] It is estimated that the amorphous nanoparticles of CoOOH showing a large surface area may contribute to such a good capacitance. Although the mixed nanoparticles of CoOOH and Co_3O_4 likely degraded to a lower specific capacitance (79 F g^{-1}) at short reaction time (1.5 h, Figure 2b and 3b), further reactions (2–4 h) restored the specific capacitances to 82 and 98 F g^{-1} for 2 and 4 h, respectively. These results imply that the nanoparticular hollow octahedra are beneficial for the charge storage. In contrast, the hollow Co_3O_4 octahedra after shell smoothening (12 h reaction, Figure 2e and 3e) revealed a poor specific capacitance of 60 F g^{-1} as a result of small surface area greatly shrunk due to the coalescence of primary nanoparticles.

A cycling life test of the Co_3O_4 hollow octahedra electrode was carried out at 2 A g^{-1} using a constant current charge-discharge experiment and the result is shown in Figure 6. The specific capacitance gradually increased up to 192 F g^{-1} at 1200 cycles and remained stable afterward, reflecting the good long-term cyclability of our Co_3O_4 electrode. Previous work[8c,9c] reported that the gradual increase in specific capacitance during the cycling may be ascribed to activation of the electrode, as electrolytes in general require a certain period of time to penetrate the entire inner space of an active electrode material. In our work, although the hollow octahedra were assembled from primary nanoparticles, we estimate that the electrolyte could not penetrate easily into the interior of hollow octahedra, thus the interior surface of hollow octahedra was unable to fully utilize for a few initial cycles. As the cycling proceeded, the electrolyte gradually penetrated into the interior of hollow octahedra, rendering Co_3O_4 more activated and finally leading to the increase in capacitance.

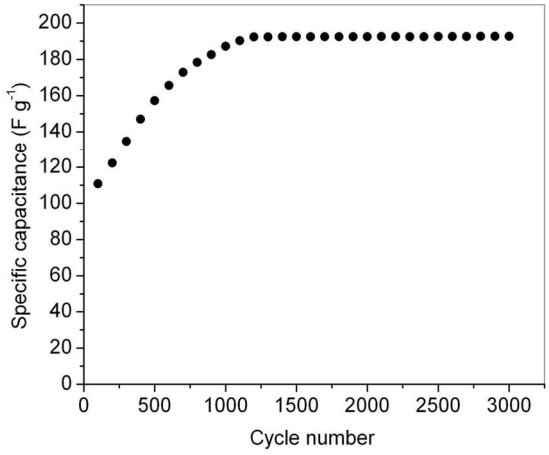

Figure 6. Cycling performance of the Co_3O_4 hollow octahedra electrode at a current density of 2 A g^{-1}.

In order to investigate the electrode stability upon cycling measurement, XRD/SEM characterization of the Co_3O_4 hollow octahedra electrodes was taken before and after cycling (Figure S5). After 3000 cycles at 2 A g^{-1}, the diffraction peaks newly appeared were labelled as triangles in Figure S5a. Although we could not precisely identify these new Co compounds, these peaks might be reasonable to stem from the highly valent Co-oxides (or Co-hydroxides) formed via the reaction routes (eqs. 2 and 3) during the cycling process. After the cycling test, the

morphological shapes of Co_3O_4 octahedra could be still retained on the whole, but the surface of electrode was likely covered with a second phase which might be originated from the new Co compounds (Figure S5b-c).

CONCLUSIONS

In summary, we developed a one-step, template-free solvothermal method to synthesize Co_3O_4 hollow octahedra. Our in-depth study revealed that newly synthesized hollow octahedra were formed through the self-assembly of primary nanoparticles and subsequent Ostwald ripening. We also found that cobalt salts used as a precursor have an effect on the Co_3O_4 morphology; Co_3O_4 nanocubes of 20-50 nm in size were obtained, rather than hollow octahedra, when the Co precursor was changed from cobalt chloride to cobalt acetate. The hollow Co_3O_4 octahedra that were prepared show a good pseudocapacitance when evaluated as an electrode material for supercapacitors. In particular, the Co_3O_4 hollow octahedra exhibited a higher specific capacitance than the Co_3O_4 nanocubes, which was attributed to lower series and diffusive resistance. A test evaluating long-term stability revealed good cycle performance of the Co_3O_4 hollow octahedra. We believe that the unique hollow structure of these Co_3O_4 octahedra may prove useful in other applications such as sensors and lithium-ion batteries.

Acknowledgements

This work was supported by the Human Resources Development program (no. 20124030200130), the Energy Technology Development program (no. 20123021010010), and the New & Renewable Energy grant (no. 20123010010160) of the Korea Institute of Energy Technology Evaluation and Planning (KETEP) Grant funded by the Korea government Ministry of Trade, Industry and Energy.

Notes and references

[a] Department of Chemical Engineering, Hanyang University, 55 Hanyangdaehak-ro, Sangnok-gu, Ansan, Kyeonggi-do 426-791, Republic of Korea

[b] State Key Laboratory of Multi-phase Complex Systems, Institute of Process Engineering, Chinese Academy of Sciences (CAS), Beijing 100190, China

[c] Department of Chemistry and Applied Chemistry and Department of Bionano Engineering, Hanyang University, 55 Hanyangdaehak-ro, Sangnok-gu, Ansan, Kyeonggi-do 426-791, Republic of Korea

[&] These authors contribute equally to the work.

[*] Corresponding authors

Email: jungho@hanyang.ac.kr (Lee), jbang@hanyang.ac.kr (Bang)

Electronic Supplementary Information (ESI) available: [SEM images of broken Co_3O_4 hollow octahedra; TEM images of the quasi-octahedra obtained after 2 h reaction; XRD pattern and SEM image of Co_3O_4 and β-$Co(OH)_2$ composite obtained when the reaction was performed with 2 M NaOH for 24 h.]. See DOI: 10.1039/b000000x/

1. (*a*) G. Wang, L. Zhang and J. Zhang, *Chem. Soc. Rev.,* 2012, **41,** 797; (*b*) Q. Lu, J. G. Chen and J. Q. Xiao, *Angew. Chem. Int. Ed.,* 2013, **52,** 2; (*c*) L. C. Haspert, E. Gillette, S. B. Lee and G. W. Rubloff, *Energy Environ. Sci.,* 2013, **6,** 2578; (*d*) M. D. Stoller and R. S. Ruoff, *Energy Environ. Sci.,* 2010, **3,** 1294; (*e*) H. Kim, M. E. Fortunato, H. Xu, J. H. Bang and K. S. Suslick, *J. Phys. Chem. C,* 2011, **115,** 20481.

2. (*a*) C. C. Hu, K. H. Chang, M. C. Lin and Y. T. Wu, *Nano Lett.,* 2006, **6,** 2690; (*b*) P. Chen, H. Chen, J. Qiu and C. Zhou, *Nano Res.,* 2010, **3,** 594.

3. (*a*) J. W. Lang, L. B. Kong, W. J. Wu, Y. C. Luo and L. Kang, *Chem. Comm.,* 2008, 4213; (*b*) J. Li, W. Zhao, F. Huang, A. Manivannan, and N. Wu, *Nanoscale,* 2011, **3,** 5103.

4. (*a*) E. J. Lee and J. H. Bang, *Mater. Lett.,* 2013, **105,** 28; (*b*) H. Wang, H. S. Casalongue, Y. Liang and H. Dai, *J. Am. Chem. Soc.,* 2010, **132,** 7472.

5. (*a*) W. Chen, R. B. Rakhi, L. Hu, X. Xie, Y. Cui and H. N. Alshareef, *Nano Lett.,* 2011, **11,** 5165; (*b*) J. Ge, H. B. Yao, W. Hu, X. F. Yu, Y. X. Yan, L. B. Mao, H. H. Li, S. S. Li and S. H. Yu, *Nano Energy,* 2013, **2,** 505.

6. Y. Yang, D. Kim, M. Yang and P. Schmuki, *Chem. Commun.,* 2011, **47,** 7746.

7. (*a*) X. Zhang, W. Shi, J. Zhu, D. J. Kharistal, W. Zhao, B. S. Lalia, H. H. Hng and Q. Yan, *Acs Nano,* 2011, **5,** 2013; (*b*) X. Lu, G. Wang, T. Zhai, M. Yu, S. Xie, Y. Ling, C. Liang, Y. Tong and Y. Li, *Nano Lett.,* 2012, **12,** 5376.

8. (*a*) C. Lin, J. A. Ritter and B. N. Popov, *J. Electrochem. Soc.,* 1998, **145,** 4097; (*b*) V. Srinivasan and J. W. Weidner, *J. Power Sources,* 2002, **108,** 15; (*c*) X. Xia, J. Tu, Y. Zhang, X. Wang, C. Gu, X. B. Zhao and H. J. Fan, *ACS Nano,* 2012, **6,** 5531; (*d*) M. J. Deng, F. L. Huang, I. W. Sun, W. T. Tsai and J. K. Chang, *Nanotechnology,* 2009, **20,** 175602; (*e*) H. Wang, L. Zhang, X. Tan, C. M. B. Holt, B. Zahiri, B. C. Olsen and D. Mitlin, *J. Phys. Chem. C,* 2011, **115,** 17599; (*f*) H. W. Wang, Z. A. Hu, Y. Q. Chang, Y. L. Chen, Z. Y. Zhang, Y. Y. Yang and H. Y. Wu, *Mater. Chem. Phys.,* 2011, **130,** 672; (*g*) Y. Wang, Z. Zhong, Y. Chen, C. T. Ng and J. Lin, *Nano Res.,* 2011, **4,** 695; (*h*) T. Y. Wei, C. H. Chen, K. H. Chang, S. Y. Lu and C. C. Hu, *Chem. Mater.,* 2009, **21,** 3228; (*i*) J. H. Kwak, Y. W. Lee and J. H. Bang, *Mater. Lett.,* 2013, **110,** 237.

9. (*a*) X. H. Xia, J. P. Tu, Y. Q. Zhang, Y. J. Mai, X. L. Wang, C. D. Gu and X. B. Zhao, *RSC Adv.,* 2012, **2,** 1835; (*b*) B. Wang, T. Zhu, H. B. Wu, R. Xu, J. S. Chen and X. W. Lou, *Nanoscale,* 2012, **4,** 2145; (*c*) X. C. Dong, H. Xu, X. W. Wang, Y. X. Huang, M. B. Chan-Park, H. Zhang, L. H. Wang, W. Huang and P. Chen, *ACS Nano,* 2012, **6,** 3206; (*d*) R. B. Rakhi, W. Chen, D. Cha and H. N. Alshareef, *Nano Lett.,* 2012, **12,** 2559; (*e*) F. Zhang, C. Yuan, X. Lu, L. Zhang, Q. Che and X. Zhang, *J. Power Sources,* 2012, **203,** 250; (*f*) Li. Yang, S. Cheng, Y. Ding, X. Zhu, Z. L. Wang and M. Liu, *Nano Lett.,* 2012, **12,** 321.

10. (*a*) X. H. Xia, J. P. Tu, Y. J. Mai, X. L. Wang, C. D. Gu and X. B. Zhao, *J. Mater. Chem.,* 2011, **21,** 9319; (*b*) X. H. Xia, J. P. Tu, X. L. Wang, C. D. Gu and X. B. Zhao, *Chem. Commun.,* 2011, **47,** 5786.

11. (*a*) Y. F. Yuan, X. H. Xia, J. B. Wu, X. H. Huang, Y. B. Pei, J. L. Yang and S. Y. Guo, *Electrochem. Commun.,* 2011, **13,** 1123; (*b*) C. Yuan, L. Yang, L. Hou, L. Shen, X. Zhang and X. W. Lou, *Energy Environ. Sci.,* 2012, **5,** 7883; (*c*) S. K. Meher and G. R. Rao, *J. Phys. Chem. C,* 2011, **115,** 15646.

12. F. Cao, D. Wang, R. Deng, J. Tang, S. Song, Y. Lei, S. Wang, S. Su, X. Yang, and H. Zhang, *CrystEngComm,* 2011, **13,** 2123.
13. (*a*) X. Wang, X. L. Wu, Y. G. Guo, Y. Zhong, X. Cao, Y. Ma and J. Yao, *Adv. Funct. Mater.,* 2010, **20,** 1680; (*b*) J. Ma and A. Manthiram, *RSC Adv.,* 2012, **2,** 3187; (*c*) J. Liu and D. Xue, *Nanoscale Res. Lett.,* 2010, **5,** 1525; (*d*) X. Wang, L. Yu, X. L. Wu, F. L. Yuan, Y. G. Guo, Y. Ma and J. N. Yao, *J. Phys. Chem. C,* 2009, **113,** 15553; (*e*) J. Liu, H. Xia, L. Lu and D. Xue, *J. Mater. Chem.,* 2010, **20,** 1506.
14. (*a*) S. Ding, T. Zhu, J. S. Chen, Z. Wang, C. Yuan and X. W. Lou, *J. Mater. Chem.,* 2011, **21,** 6602; (*b*) C. Y. Cao, W. Guo, Z. M. Cui, W. G. Song and W. Cai, *J. Mater. Chem.,* 2011, **21,** 3204; (*c*) G. Zhang, L. Yu, H. E. Hoster and X. W. Lou, *Nanoscale,* 2013, **5,** 877; (*d*) W. Du, R. Liu, Y. Jiang, Q. Lu, Y. Fan and F. Gao, *J. Power Sources,* 2013, **227,** 101.
15. (*a*) Y. Cao, F. Yuan, X. Zhang and Y. Chen, *J. Nanosci. Lett.,* 2012, **2,** 4; (b) X. W. Lou, L. A. Archer and Z. Yang, *Adv. Mater.,* 2008, **20,** 3987; (*c*) J. H. Bang and K. S. Suslick, *Adv. Mater.,* 2009, **21,** 3186; (*d*) J. Hu, M. Chen, X. Fang and L. Wu, *Chem. Soc. Rev.,* 2011, **40,** 5472.
16. (*a*) X. P. Shen, H. J. Miao, H. Zhao and Z. Xu, *Appl. Phys. A,* 2008, **91,** 47; (*b*) T. He, D. Chen, X. Jiao and Y. Wang, *Adv. Mater.,* 2006, **18,** 1078; (*c*) J. W. Kim, S. H. Choi, P. T. Lillechei, S. H. Chu, G. C. King and G. D. Watt, *Chem. Commun.,* 2005, 4101.
17. Z. Fei, S. He, L. Li, W. Ji and C. T. Au, *Chem. Commun.,* 2012, **48,** 853.
18. V. Pralong, A. Delahaye-Vidal, B. Beaudoin, B. Gérand and J. M. Tarascon, *J. Mater. Chem.,* 1999, **9,** 955.
19. L. K. Avramoy, *Thermochim. Acta,* 1977, **19,** 147.
20. S. Kittaka, N. Uchida, I. Miyashita and T. Wakayama, *Colloids Surf.,* 1989, **37,** 39.
21. C. H. Chen, S. F. Abbas, A. Morey, S. Sithambaram, L. P. Xu, H. F. Garces, W. A. Hines and S. L. Suib, *Adv. Mater.,* 2008, **20,** 1205.
22. (*a*) S. Ayyappan, R. S. Gopalan, G. N. Subbanna and C. N. R. Rao, *J. Mater. Res.,* 1997, **12,** 398; (*b*) Y. Ye, F. L. Yuan, L. Zhou and H. Huang, *Key Eng. Mater.,* 2007, **334-335,** 1145.
23. G. Furlanetto and L. Formaro, *J. Colloid Interface Sci.,* 1995, **170,** 169.
24. Y. Dong, K. He, L. Yin and A. Zhang, *Nanotechnology,* 2007, **18,** 435602.
25. (*a*) R. Q. Song and H. Cölfen, *Adv. Mater.,* 2010, **22,** 1301; (*b*) Y. B. Cao, J. M. Fan, L. Y. Bai, P. Hu, G. Yang, F. L. Yuan and Y. F. Chen, *CrystEngComm,* 2010, **12,** 3894; (*c*) J. Fang, B. Ding and H. Gleiter, *Chem. Soc. Rev.,* 2011, **40,** 5347; (*d*) L. Zhou and P. O'Brien, *J. Phys. Chem. Lett.* 2012, **3,** 620; (*e*) L. Liu, H. Liang, H. Yang, J. Wei and Y. Yang, *Nanotechnology,* 2011, **22,** 015603.
26. A. Querejeta-Fernández, J. C. Hernández-Garrido, H. Yang, Y. Zhou, A. Varela, M. Parras, J. J. Calvino-Gamez, J. M. González-Calbet, P. F. Green and N. A. Kotov, *ACS Nano,* 2012, **6,** 3800.
27. Z. L. Wang, *Part. Part. Syst. Charact.,* 2001, **18,** 142.
28. J. F. Banfield, S. A. Welch, H. Zhang, T. T. Ebert and R. L. Penn, *Science,* 2000, **289,** 751.
29. (*a*) P. Hu, L. Yu, A. Zuo, C. Guo and F. Yuan, *J. Phys. Chem. C,* 2009, **113,** 900; (*b*) Z. Chen, Z. Geng, M. Shi, Z. Liu and Z. Wang, *CrystEngComm,* 2009, **11,** 1591; (*c*) J. X. Cui, W. S. Wang, L. Zhen, W. Z. Shao and Z. L. Chen, *CrystEngComm,* 2012, **14,** 7025; (*d*) B. Liu and H. C. Zeng, *Small,* 2005, **1,** 566.
30. (*a*) H. G. Liao, L. Cui, S. Whitelam and H. Zheng, *Science,* 2012, **336,** 1011; (*b*) J. M. Yuk, J. Park, P. Ercius, K. Kim, D. J. Hellebusch, M. F. Crommie, J. Y. Lee, A. Zettl and A. P. Alivisatos, *Science,* 2012, **336,** 61.
31. K. Gao, Z. Chai, G. Xu, X. Wang and C. Wang, *Nano Res.,* 2009, **2,** 565.
32. (*a*) E. Hosono, S. Fujihara, I. Honma, M. Ichihara and H. Zhou, *J. Power Sources,* 2006, **158,** 779; (*b*) H. Zheng, F. Tang, M. Lim, T. Rufford, A. Mukherji, L. Wang and G. Lu, *J. Power Sources,* 2009, **193,** 930.

Table of Contents Graphic

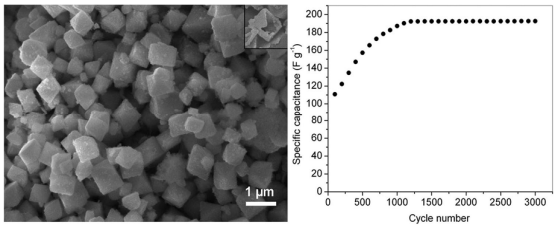

Hollow Co_3O_4 octahedra, synthesized through a new solvothermal method, exhibited a charge storage capacity of 192 F g^{-1} with good long-term cycleability.